Case Study

Seismic Fragility Analysis of Base-Isolated Structures Based on Response Surface Method

Chao Luo, Ph.D.[1]; Hao Wang, Ph.D.[2]; Xiaoxia Guo[3]; Feiyu Wang[4]; Kexin Tao[5]; and Huaiping Feng[6]

Abstract: Base-isolated structures face a risk of damage under the action of earthquakes, and base isolation devices may be susceptible to damage during severe earthquakes. This study proposed an approach based on the response surface method to assess the base-isolated structures' seismic fragility and investigated the reliability and effectiveness of the base-isolation technique. Three performance levels and corresponding performance criteria for general base-isolated reinforced concrete structures were specified. The proposed seismic fragility assessment approach fully considered the uncertainty of the base-isolated structures and ground motions. Uncertainty parameters of the superstructure and base isolators were characterized, and parametric sensitivity analysis of the base-isolated structure was carried out. Moreover, the seismic fragility evaluation method of base-isolation systems was studied, and a simplified evaluation equation was introduced. The proposed response surface-based method's accuracy and efficiency were also compared with the Monte Carlo method. An actual project was taken as an example to illustrate the proposed approach. The failure probabilities of the base-isolated structure under various seismic intensity levels were calculated, and the seismic fragility curves were plotted. It indicated that the base-isolated structure could achieve the performance objectives of maintaining operation under minor earthquakes, guaranteeing life safety under moderate earthquakes, and preventing collapse under severe earthquakes. However, the seismic isolation bearings could still have large displacements under severe earthquakes. Furthermore, the seismic fragility analysis of the base-isolated and nonisolated structures was compared. It showed that the base isolation technique significantly reduced the damage probability of the superstructure under various intensity levels and effectively prevented the superstructure from entering a serious damage state. The proposed seismic fragility analysis approach and a large amount of computational data could provide a significant engineering application value for similar reinforced concrete structures and a reference value for the design of base-isolated structures. **DOI: 10.1061/AJRUA6.RUENG-1020.**

Author keywords: Base isolation; Seismic fragility; Response surface method; Damage probability; Randomness.

Introduction

In the past two decades, the seismic base-isolation technique has been widely used in structural design for its excellent performance in mitigating seismic response. However, the base-isolation structure is still exposed to the risk of earthquake damage. On the one hand, the building response may deviate from the deterministic seismic response analysis due to the presence of uncertainties in the seismic loads and structures. On the other hand, the reliability of seismic isolators under earthquakes, especially beyond design basis earthquakes, is paramount because the displacement of the isolation layer is large. Therefore, it is significant to analyze the seismic fragility of base-isolated structures.

Many researchers perform seismic fragility analysis on base-isolated structures, including critical facilities, buildings, and bridges. The analytical methods are more feasible in the absence of seismic damage data because the empirical methods require seismic damage data from actual earthquakes. Therefore, seismic fragility analysis research based on analytical methods has prevailed in recent years. Perotti et al. (2013) analyzed the seismic fragility of base-isolated buildings in nuclear power plants (NPP) using the response surface method (RSM) and Monte Carlo simulation (MCS) method. Saha et al. (2016) transferred the study subject to the base-isolated liquid storage tank in the same way. Salimi Firoozabad et al. (2015) experimentally verified the numerical results of the fragility of the base-isolated NPP piping system. Alhan and Gavin (2005) used the MCS approach to determine the fragility of base isolation under critical equipment. Castaldo et al. (2015) evaluated the seismic fragility of friction pendulum isolators using the Latin Hypercube Sampling (LHS) method. Long et al. (2015) conduct seismic fragility analysis of an isolated continuous girder bridge using the RSM. Xiao et al. (2020) proposed an improved RSM for fragility analysis of base-isolated structures, considering the correlation of seismic demands on the structural components.

[1]State Key Laboratory of Mechanical Behavior and System Safety of Traffic Engineering Structures, Shijiazhuang Tiedao Univ., Shijiazhuang 050043, China. ORCID: https://orcid.org/0000-0003-3166-7644. Email: luochao@stdu.edu.cn

[2]State Key Laboratory of Mechanical Behavior and System Safety of Traffic Engineering Structures, Shijiazhuang Tiedao Univ., Shijiazhuang 050043, China (corresponding author). ORCID: https://orcid.org/0000-0002-7463-1433. Email: wanghao@stdu.edu.cn

[3]School of Civil Engineering, Shijiazhuang Tiedao Univ., Shijiazhuang 050043, China. Email: 1202101167@student.stdu.edu.cn

[4]School of Civil Engineering, Shijiazhuang Tiedao Univ., Shijiazhuang 050043, China. Email: 172917473@qq.com

[5]School of Civil Engineering, Shijiazhuang Tiedao Univ., Shijiazhuang 050043, China. Email: 983634590@qq.com

[6]Professor, State Key Laboratory of Mechanical Behavior and System Safety of Traffic Engineering Structures, Shijiazhuang Tiedao Univ., Shijiazhuang 050043, China. ORCID: https://orcid.org/0000-0003-2435-1027. Email: fenghuaiping@stdu.edu.cn

Note. This manuscript was submitted on October 19, 2022; approved on March 10, 2023; published online on May 19, 2023. Discussion period open until October 19, 2023; separate discussions must be submitted for individual papers. This paper is part of the ***ASCE-ASME Journal of Risk and Uncertainty in Engineering Systems, Part A: Civil Engineering***, © ASCE, ISSN 2376-7642.

Among recent research, improved MCS methods are commonly used seismic fragility analysis methods for base-isolated structures. The direct MCS method is one of the most accurate analytical methods in reliability analysis and is often used to examine the accuracy of other reliability methods. However, the direct MCS method requires a considerable amount of simulations to obtain a reliable estimate, especially for the low probability of failure (Peeranan 2004). Nonlinear analysis is necessary when conducting seismic fragility of base-isolated structures because the isolators may exhibit a strong nonlinear behavior. Therefore, it is computationally impractical to use the direct MCS method for seismic fragility analysis of base-isolated structures (Franchin et al. 2003). Hence, many scholars adopt the improved MCS method, such as improved sampling methods and RSM-based MCS methods. The response surface method (RSM) provides an efficient option in the field of structural reliability analysis (Peeranan 2004). The basic idea of the RSM is to replace the real complex limit state function with a simple function containing unknown parameters and transform the complex implicit reliability problem into a relatively simple explicit reliability problem. The RSM offers many advantages: (1) it is a nonintrusive method that can be easily combined with deterministic structural analysis programs; and (2) it shows a good application prospect in the fragility analysis field of large and complex structures, because it dramatically reduces the time of nonlinear finite-element analysis. However, conventional RSM builds the relationship between the structural random variables and building seismic response through an explicit function: develop one metamodel to replace the finite-element model. When the uncertainty of ground motion is taken into account in this way, a suite of ground motions corresponding to a specific level of intensity are selected randomly and matched with randomly selected response surface metamodels, like Approach 2 in Peeranan (2004). As a result, the number of response surface models is the same as the number of ground motions in the suite. If the uncertainty of ground motion needs to be fully considered, a large number of trials may be required, so the computational cost of seismic fragility analysis by this method is still very high. Therefore, it is essential to study the improved RSM and verify it on the seismic isolation structure.

This study proposed an improved RSM-based simulation approach to assess the seismic fragility of the base-isolated reinforced concrete (RC) structures. In this approach, both the uncertainties of the base-isolated structures and the ground motions were considered. First, the damage criteria for general base-isolated RC buildings were suggested. Second, the uncertainties of the base-isolated structures and the ground motions were characterized. Parameter sensitivity analyses were performed to study the sensitivity of the uncertainty parameters of base-isolated structures. The uncertainty of ground motions was fully considered, and seismic intensity was incorporated as an uncertain parameter by constructing dual response surfaces. Third, an actual RC structural project was taken as an example to illustrate the proposed approach. Dual response surface models of the base-isolated structure were built, including the structural uncertainty parameters and the peak ground motion acceleration (PGA). The efficiency and accuracy of the proposed RSM were verified by the direct MCS method. The approximated equations to assess the seismic fragility of base-isolated systems were studied. Last, the failure probability of the base-isolated structure under various seismic levels was calculated, and particular emphasis was laid on the seismic performance under severe earthquakes. The seismic fragility of the base-isolated system was analyzed and compared with its nonisolated counterpart to investigate the reliability and effectiveness of base-isolation techniques.

Damage Criteria of Base-Isolated RC Structures

The peak interstory drift ratio (PIDR) can characterize the structural plastic behavior when encountering severe earthquakes and sensitively respond to the change in structural stiffness. The maximum displacement of the isolation layer (MDIL) can reflect the deformation degree of seismic isolators. Thus, they are identified as engineering demand parameters (EDP) for base-isolated structures. Three performance levels of base-isolated RC structures are defined as operational, life safety (LS), and collapse prevention (CP). ASCE 41-17 (ASCE 2014) states that the seismically isolated structure should remain essentially elastic when subjected to basic safety earthquake 1 (BSE-1), and the inelastic response of the lateral force-resisting members of the superstructure should be limited to 1/3 of the nonlinear response limit of the nonisolated structure. The superstructure should be regarded as an elastic system under design basic earthquakes, thus the performance criteria of the PIDR for the operational limit state corresponds to the elastic deformation limit of RC structures. And the inelastic deformation limit of RC structures is defined as the CP limit state, because the inelastic deformation limit controls the RC structure from collapsing under major earthquakes. And the performance criteria for the LS limit state is 1/3 of that for the CP limit state, considering that the inelastic response of the lateral force-resisting superstructure system is limited to about 1/3 of a comparable fixed-base structure for design major earthquakes. According to the Chinese code for seismic design of buildings (GB 50011-2010) (MOHURD 2016), the elastic and inelastic deformation limit of RC structures is 1/550 and 1/50, respectively. Therefore, the threshold of the PIDR for the operational, LS, and CP limit states are 1/550, 1/150, and 1/50, respectively (Wang et al. 2020). The MDIL of each limit state is defined by the isolators' shear strain, which is presented γ in Table 1. China's standard for seismic isolation design of building (SAPRC 2021) stipulates that for the seismic isolation structure using only rubber isolation bearings, the horizontal shear strain can be taken as follows: 100% for basic fortification earthquakes, 250% for major earthquakes, and 400% for very rare earthquakes. So 100% γ, 250% γ, and 400% γ are set as the limit values of the operational, LS, and CP limit states, respectively (Wang et al. 2020). Three performance levels and corresponding performance criteria are specified, as shown in Table 1.

The limit state function of nonisolated RC structures is constructed as

$$g_i(\mathbf{X}) = \theta_i - \theta_{\max}(\mathbf{X}) \tag{1}$$

where $\mathbf{X}$ = random variables vector; $g_i(\mathbf{X})$ = performance function with respect to ith limit state; θ_i denotes the PIDR limit with respect to ith limit state; and $\theta_{\max}(\mathbf{X})$ denotes the PIDR of the RC structure.

The limit state functions of base-isolated RC structures are defined as

$$\begin{aligned} g_i(\mathbf{X}) &= \theta_i - \theta_{\max}(\mathbf{X}) \\ g_i(\mathbf{X}) &= \delta_i - \delta_{LRB}(\mathbf{X}) \end{aligned} \tag{2}$$

where δ_i denotes the MDIL limit with respect to ith limit state; and $\delta_{LRB}(\mathbf{X})$ denotes the MDIL.

Table 1. Performance levels of base-isolated reinforced concrete structures

Demand parameters	Operational	Life safety	Collapse prevention
PIDR	1/550	1/150	1/50
MDIL	100% γ	250% γ	400% γ

RSM-Based Seismic Fragility Analysis Approach

Seismic fragility provides the value of the conditional probability of a particular damage state being exceeded given a particular instance of a hazardous scenario (Saha et al. 2016). The seismic fragility of base-isolated structures can be represented as a conditional probability

$$F_R(y) = P[D \geq C|IM = y] \tag{3}$$

where D denotes the seismic demands; C denotes the structural capacity; and $IM = y$ denotes the specific level of a selected seismic intensity measure (IM).

Assuming that the seismic response of the structure exceeds the limits, the structure is considered to have failed. If i limit states are defined, the failure probability with respect to ith limit state at each intensity level can be expressed as

$$PF_{ij} = P(LS_i|IM = y_j) = P(EDP \geq x_i|IM = y_j) \tag{4}$$

where PF_{ij} describes the failure probability with respect to ith limit state at the ith IM level; LS_i denotes ith limit state; EDP = seismic demand parameters; and x_i = limit value of seismic responses with respect to ith limit state.

Once the probability distribution of random variables $\mathbf{X} = (X_1, X_2, \ldots, X_n)$ is characterized, the probability of exceeding a specific limit state can be expressed as

$$PF_{ij} = P(g_i(\mathbf{X}) \leq 0|IM = y_j) = \int_{g_i(X|IM=y_j)|\leq 0} f_{\mathbf{X}}(x)dx \tag{5}$$

The integral could be computed by the straightforward MCS method, but it would cost massive computation time for base-isolated systems (Franchin et al. 2003). In this study, the RSM-based MCS method is explored to assess the seismic fragility of base-isolated structures. The actual limit state function $g(\mathbf{X})$ is replaced by an explicit function, namely the response surface function (RSF). The RSF needs to have sufficient ability to reflect the true limit states and keep the form as simple as possible with few coefficients to be determined to reduce the computation workload. Using quadratic polynomials with cross terms to represent RSF has the advantages of low computational cost, high computational stability, and can reflect the nonlinearity of structural seismic responses (Peeranan 2004). Thus, in this paper, the metamodel representation uses a quadratic polynomial with cross terms

$$\hat{Z} = \hat{g}(\mathbf{X}) = a + \sum_{i=1}^{n} b_i X_i + \sum_{i=1}^{n} c_i X_i^2 + \sum_{i=1}^{n-1} \sum_{j=i+1}^{n} d_{ij} X_i X_j + \varepsilon \tag{6}$$

where a, b_i, c_i, and d_{ij} = polynomial coefficients; n = number of variables $\mathbf{X}$; and ε = random error.

The polynomial coefficients in the RSF are determined through experimental design. First, select a series of design points in the design space, namely, determine a series of random variables combinations. The experimental design scheme of the structural input random variables adopts the central composite design (CCD) strategy. The number of coefficients necessary for CCD is $2^n + 2n + 1$, including one center point, 2^n factorial points, and $2n$ axial points. The initial design center is assumed at the mean values of the random variables $\mathbf{x}_M = (\mu_{X_1}, \mu_{X_2}, \ldots, \mu_{X_n})$. The cube points are selected by a complete 2^n factorial design, namely $(x_{M1} \pm 2\sigma_1, \ldots, x_{Mi} \pm 2\sigma_i, \ldots, x_{Mn} \pm 2\sigma_n)$. The axial points are selected on each design variable's axis at a distance α from the design center $(x_{M1}, \ldots, x_{Mi} \pm \alpha\sigma_i, \ldots, x_{Mn})$. Make $\alpha = \sqrt[4]{2^n} = \sqrt[4]{2^5}$ so that the CCD is rotatable. When dealing with the uncertainty of ground motions, divide ground acceleration records into three batches, the intensity measure PGA of each batch is set to minor, basic, and severe seismic intensity levels, respectively, and arbitrary combination with structural random variables forms the experimental design points. Then, calculate the seismic demands, PIDR, and MDIL, corresponding to each design point through nonlinear time-history analysis. The seismic demands and the value of design points construct a set of linear equations. Use the least square regression method to fit the functional relationship between structural input variables and seismic demands.

The dual response surface concept is introduced in this RSM-based approach (Buratti et al. 2010; Franchin et al. 2003; Peeranan 2004) to incorporate the uncertainty of ground motions into the response surface model. This approach assumes that the seismic responses follow a normal distribution. The dual response surface method uses the mean response metamodel to achieve the target fit and the standard deviation response metamodel to ensure that the fitted function is robust to uncontrollable factors. The IM is treated as an uncertainty parameter in addition to the structural uncertainty parameters, which indicates an additional dimension is added to plot the seismic response and a vector of input parameters. Adding a random variable IM will increase the workload of experimental design, but the response surface developed is not specific to a certain level of seismic intensity. Thus, the seismic fragilities at various seismic intensity levels can be analyzed through one response surface function, which is much more efficient.

The response surface metamodels for predicting the mean and the standard deviation of structural responses are

$$\hat{y}_\mu = g(\mathbf{x}, IM) \tag{7}$$

$$\hat{y}_\sigma = h(\mathbf{x}, IM) \tag{8}$$

where $g(\mathbf{x}, IM)$ and $h(\mathbf{x}, IM)$ = response surface metamodels for predicting the mean and standard deviation of the seismic responses due to a suite of ground motions, respectively. $g(\mathbf{x}, IM)$ and $h(\mathbf{x}, IM)$ can apply the metamodel representation [Eq. (6)].

Assuming that the structural response follows a normal distribution, the overall response surface model is

$$\hat{y} = g(\mathbf{x}, IM) + N[0, h(\mathbf{x}, IM)] \tag{9}$$

To test the fitting degree of the response surface function to the response value, the modified multiple correlation coefficient can be used as the evaluation index. The closer the modified multiple correlation coefficient is to 1, the better the fit of the regression equation is

$$R_a^2 = 1 - \left(\frac{k-1}{k-p}\right)\frac{SSE}{SST} = 1 - \frac{k-1}{k-p}(1 - R^2) \tag{10}$$

where R_a = modified multiple correlation coefficient; k = number of test points of the response surface model; p = number of parameters to be estimated; and R = multiple correlation coefficients

$$R^2 = \frac{SSR}{SST} = 1 - \frac{SSE}{SST} \tag{11}$$

where SST = sum of squares for total; SSE = sum of squares due to error; and SSR = sum of squares due to regression.

Apply the MCS method to the approximated model. Note that the experimental design is based on both structural uncertainty parameters and seismic intensity parameter. In each Monte Carlo simulation, fix the intensity measure parameter at a certain level while varying the structural parameters according to their probability

distribution. Then, the simulations can obtain the damage probabilities conditioned on that particular intensity level. Repeat the process at various seismic intensity levels, and then the seismic fragility curves can be plotted.

Numerical Example

Modeling of the Base-Isolated Structure

The seismic performance of an actual RC frame structure is assessed using the RSM-based approach. This RC frame structure is located in Kashgar, China. According to the Chinese code for seismic design of buildings (MOHURD 2016), the building site is Class II, the seismic design grouping is Group III, and the characteristic period Tg of seismic design response spectrum is taken as 0.45 s. The basic seismic design intensity PGA is 0.3 g. The building has eight floors and a total construction area of 9,500 m^2. The standard structural plan is shown in Fig. 1. The total height of the building is 29.7 m, the ground floor is 3.9 m high, the 2nd–6th floors are 3.6 m high, the 7th floor is 4.2 m high, and the 8th floor is 3.6 m high. The cross-sectional dimensions of the frame columns are 600×600 mm^2, 650×650 mm^2, and 700×700 mm^2 for the 1st–8th floors. The concrete strength of the 1st–2nd floors is C40, the 3rd–8th floors is C30, and the floor main beam section size is 350×620 mm^2 and 350×820 mm^2, the secondary beam section size is 250×550 mm^2 and 250×500 mm^2. The primary and secondary beam concrete strength grade is C30. The total mass of the building is about 14,061 tons, and the basic information of each story is shown in Table 2.

The existing building needs to be strengthened due to the revision of China's seismic design code, and the function of the building must not be affected during the construction. Therefore, the base isolation technique is used to rehabilitate the structure.

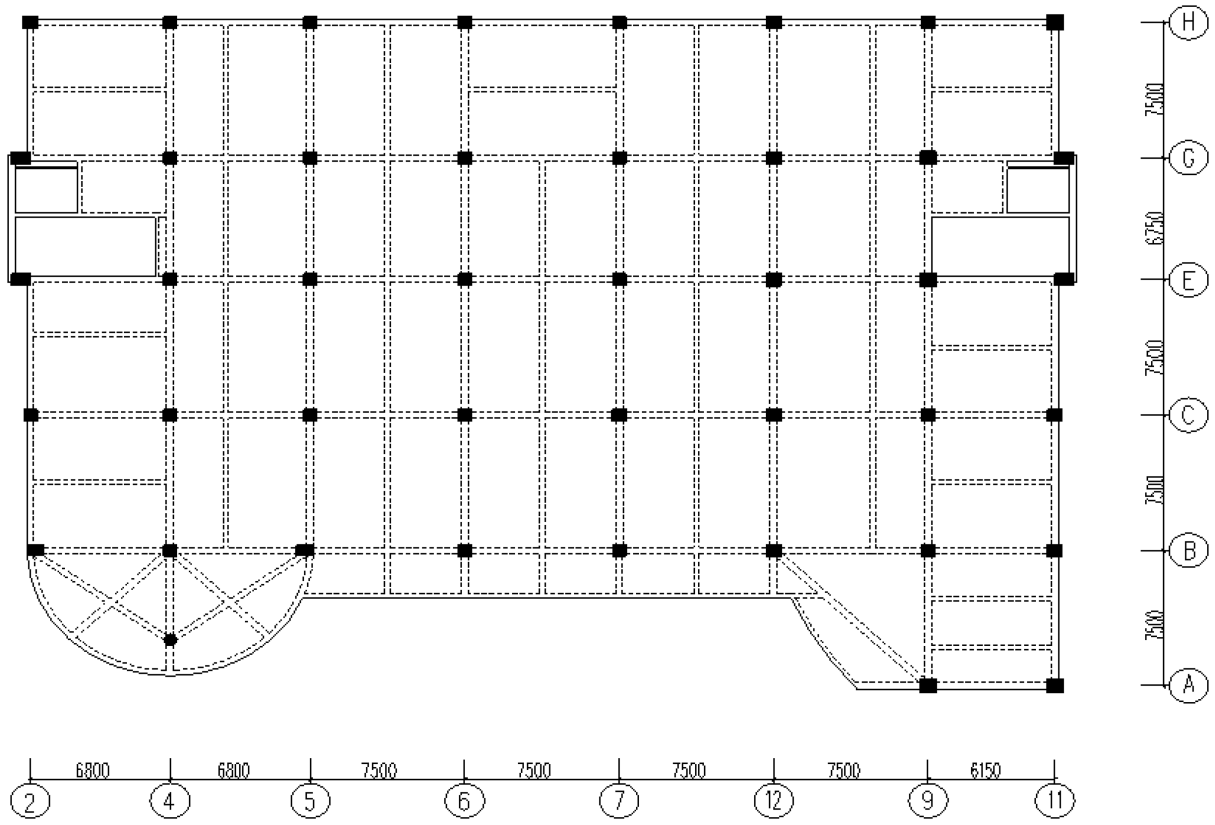

Fig. 1. Standard structural floor plan.

Table 2. Basic design values of the nonisolated structure

Story No.	Storey height (m)	Mass (t)	Long side direction		Short side direction	
			Stiffness (kN/mm)	Storey shear force (kN)	Stiffness (kN/mm)	Storey shear force (kN)
8	3.6	155	1.09×10^5	115	1.18×10^5	121
7	4.2	941	3.63×10^5	784	3.69×10^5	778
6	3.6	2,030	8.28×10^5	2,085	8.03×10^5	1,849
5	3.6	1,996	9.11×10^5	3,225	8.66×10^5	2,764
4	3.6	2,177	9.45×10^5	4,261	8.86×10^5	3,584
3	3.6	2,247	9.93×10^5	5,061	9.18×10^5	4,254
2	3.6	2,324	1.12×10^6	5,576	1.03×10^6	4,657
1	3.9	2,191	1.73×10^6	5,772	1.56×10^6	4,810

Table 3. Design mechanical properties of lead rubber bearings

Isolator type	Datum pressure (MPa)	Long-term load (kN)	Vertical stiffness, Kv (kN/mm)	Initial stiffness, K1 (kN/mm)	Postyield stiffness, Kd (kN/mm)	Equivalent horizontal stiffness, Kh (kN/mm)	Yield strength, Qd (kN)	Damping, Heq (%)
LRB700	15	5,603	3,157	14.213	1.093	1.643	76	20.4
LRB800	15	7,275	3,671	16.447	1.265	2.052	123	23.1
LRB900	15	9,202	4,260	18.511	1.424	2.337	160	23.5

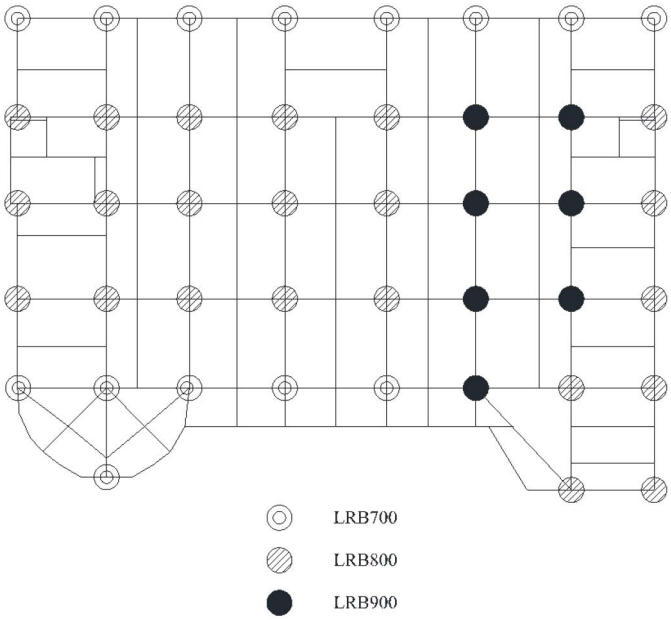

Fig. 2. Floor plan of isolation bearings.

The performance objective of the base-isolated structure is to reduce the seismic design intensity PGA of the superstructure to 0.15 g. Forty-three lead rubber bearings (LRB) were installed at the upper column section of the first floor. The main mechanical properties of the bearings are shown in Table 3 and the plane layout is shown in Fig. 2. The total horizontal stiffness of the 43 isolation bearings is 84 kN/mm, and the isolation bearings can withstand the gravity transmitted downward by the upper structure.

The stress-strain relation of concrete is the Mander confined concrete stress-strain model. The constitutive model of confined concrete adopts a multistage linear dynamic enhanced elastoplastic model that obeys the von Mises yield criterion. The seismic isolators are simulated with spring-damped elements, and a bilinear model is assumed for the seismic isolation bearing. The damping model of the superstructure uses Rayleigh damping, and the damping of the isolator bearings is achieved by attaching 20% damping to the isolation elements.

The modal analysis of the base-isolated and nonisolated structures was carried out by the Block Lanczo method, and the natural periods of the structures before and after seismic isolation are shown in Table 4. The structural stiffness in the long- and short-side directions is relatively close, so the ground motion is input along the short-side direction during the time history analysis.

Uncertainties in Base-Isolated Structures

The uncertainty parameters of base-isolated structures are grouped into the superstructure's uncertainty parameters and the seismic isolators' uncertainty parameters. The latter ones are paid more attention to because this study's main objective is to study the isolation's influence on the structure. It would require massive computation time if the uncertainty parameters exceed five, noting that the number of nonlinear time-history analyses required to solve the unknown coefficients is $2^n + 2n + 1$ for a response surface function with n random variables. Thus, the study scope is limited to aleatoric uncertainties, and the most influential parameters are first screened out through sensitivity analysis.

Table 4. Natural periods of the base-isolated and nonisolated structures

Modal order	Nonisolated structure	Isolated structure
First order	1.27 s	2.74 s
Second order	1.21 s	2.57 s
Third order	1.05 s	2.38 s

The uncertainty factors that could affect structural performance have been studied by many researchers (Castaldo et al. 2015; Celik and Ellingwood 2010; Han et al. 2014; Kwon and Elnashai 2006; Mishra and Chakraborty 2013; Perotti et al. 2013; Saha et al. 2016). The uncertain parameters selected can primarily reflect the strength, stiffness, deformation capacity, and energy dissipation characteristics of the base-isolated structure. The uncertainty parameters of RC superstructures are identified as concrete compressive strength, concrete elastic modulus, and bulk density. The uncertainty of the concrete compressive strength can characterize the uncertainty of the structure's load-bearing capacity under various damage states. This paper assumes that the average compressive strength of concrete is 1.25 times the specified compressive strength, and the coefficient of variation is 18%, referring to the research results of Ellingwood (ASCE 1980). The concrete elastic modulus is an important parameter to characterize the structure's stiffness. It reflects the deformation performance of the structure to a certain extent. This paper assumes that the concrete elastic modulus is normally distributed, the mean value is the design value of the elasticity modulus, and the coefficient of variation is 10%, referring to the research results of Li and Chen (2004). Errors in material manufacturing and the construction process may cause the density of materials and dimensions of members in the actual project to differ from the theoretical design values, resulting in structural masses that do not match the design values. The structural mass directly affects the structure's dynamic properties, so this paper assumes the dead load obeys a normal distribution with a mean value of 1.05 times standard value of dead load, and a coefficient of variation of 10%, referring to load criteria for American national standard A58 (ASCE 1980).

The uncertainty parameters of the seismic isolators are identified as the postyield stiffness and the yield strength because they can better characterize the performance of the seismic isolation bearing under strong earthquakes. The postyield stiffness of the rubber bearing is related to the rubber's shear deformation, the rubber's effective bonding area, and the rubber layer's thickness. Chinese rubber bearing product standards (GAQSIQ 2006) provide that rubber bearings are divided into two categories, S-A and S-B, according to the allowable deviation of shear performance. The allowable deviation of a single specimen's shear deformation is $\pm 15\%$ and

Table 5. Structural uncertainties of base-isolated reinforced concrete structures

Substructure	Random parameters	Mean	COV	Distribution
Superstructure	Concrete elastic modulus, E_c	Initial design value	0.10	Normal
	Concrete compression strength, $f_{cu,k}$	1.25 specified compressive strength	0.18	Normal
	Bulk density, γ_w	$1.05G_k$ (standard value of dead load)	0.10	Normal
Lead rubber bearings	Postyield stiffness, K_d	Initial design value	0.15	Normal
	Yield strength, Q_d	Initial design value	0.15	Normal

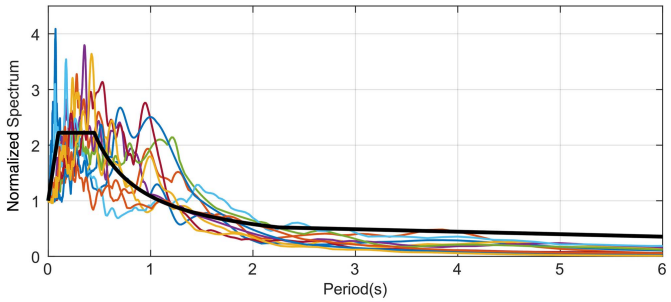

Fig. 3. Response spectrum of 10 acceleration records for the sensitivity analysis.

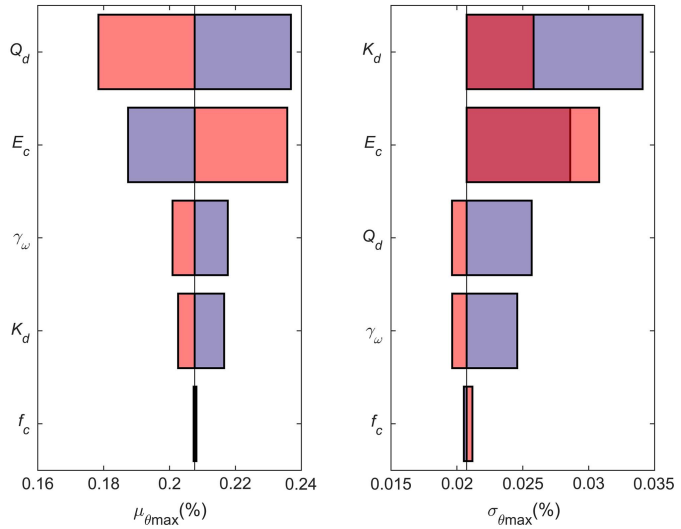

Fig. 4. Parameter sensitivities of the PIDR at frequent earthquake level.

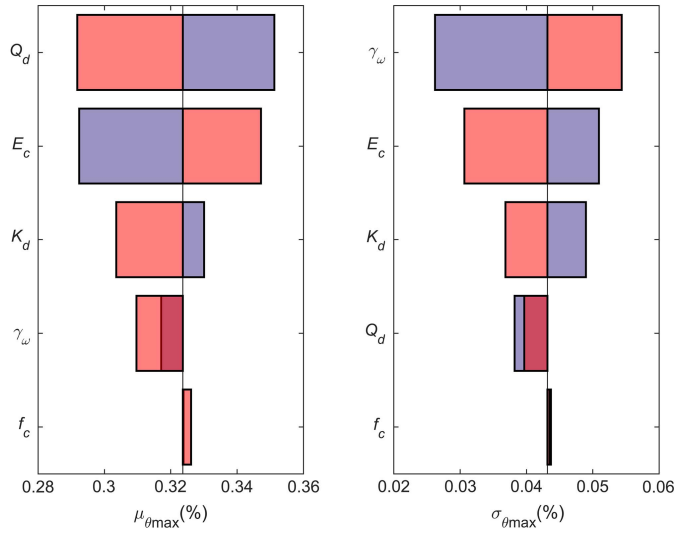

Fig. 5. Parameter sensitivities of the PIDR at design basic earthquake level.

±25% for S-A and S-B categories, respectively, and for a batch of specimens is ±10% and ±20%. In this paper, it is assumed that the horizontal postyield stiffness of the isolation bearing conforms to a normal distribution, with the mean value being the initial design value and the coefficient of variation being 15%. The yield strength of the rubber bearing is related to many factors such as axial force, lead-core size, and bearing manufacturing conditions. This paper refers to Mishra's study (Mishra and Chakraborty 2013), assuming that the yield strength of the rubber bearing is normally distributed, the mean value is the initial design value of the yield strength, and the coefficient of variation is 15%. Statistical descriptions of structural uncertainties are shown in Table 5 (Wang et al. 2020), assuming that they are independent of each other.

The sensitivity analysis is conducted to evaluate each uncertainty parameter's influence on structural seismic performance. The sensitivity analysis follows these steps: (1) Perturb a specific random variable, whereas other random variables remain 50% probability quantile. The perturbations boundary is set at 10% and 90% probability quantiles. Then, select 10 acceleration records from NGA-West2 to conduct nonlinear time-history analysis at three seismic intensity levels: frequent earthquake, design basic earthquake, and severe earthquake. The acceleration records are shown in Fig. 3. Estimate the mean and standard deviation of the structural responses using the maximum likelihood method, assuming that the structural response conforms to a normal distribution, and observe the magnitude of change in the structural responses; and (2) Perturb the random variables one by one, then compare the sensitivity of all parameters according to the magnitude of change in the structural responses.

Parameter sensitivities of the PIDR are shown by tornado diagrams from Figs. 4–6, and parameter sensitivities of the MDIL are shown from Figs. 7–9. In the above figures, orange represents the 10th percentile value of the random variable, purple represents the 90th percentile value of the random variable, and red represents the overlap between the two.

The sensitivity analysis showed that the concrete elastic modulus, the bulk density, the isolators' yield strength, and the isolators' postyield stiffness are the most influential parameters on the PIDR and the MDIL, and the concrete compression strength has the least effect. Therefore, these four parameters are identified as the uncertainty parameters for the seismic fragility analysis.

Uncertainty of Earthquake Loadings

The PGA provides a high correlation with the structural response of base-isolated structures (Box and Wilson 1951). Also, the intensity

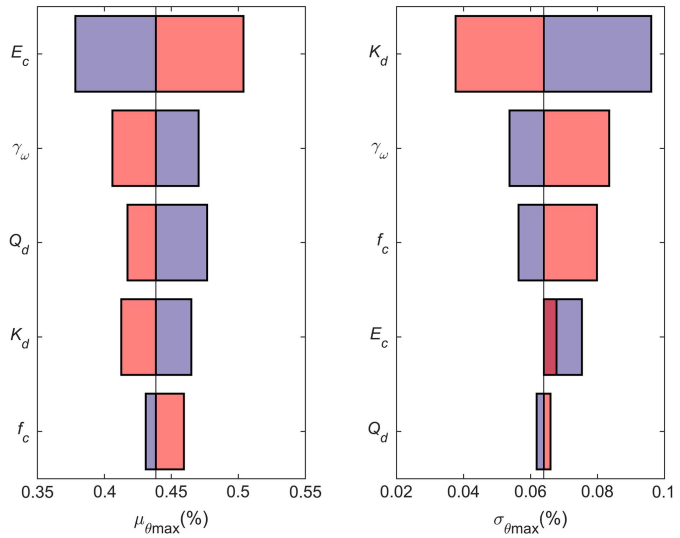

Fig. 6. Parameter sensitivities of the PIDR at severe earthquake level.

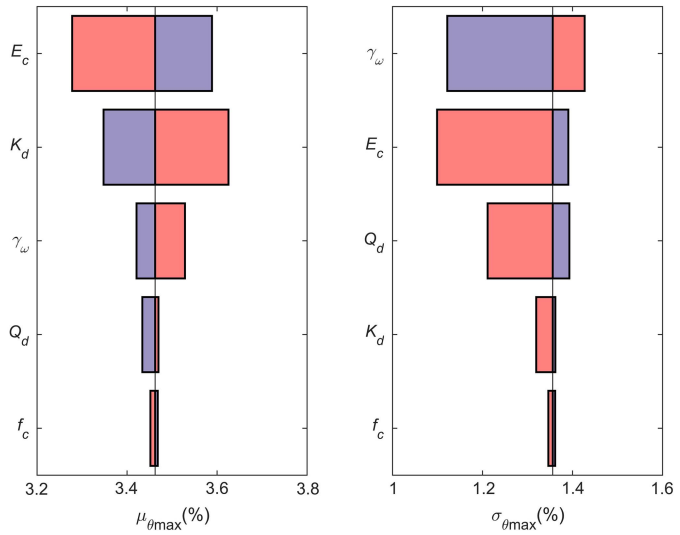

Fig. 7. Parameter sensitivities of the MDIL at frequent earthquake level.

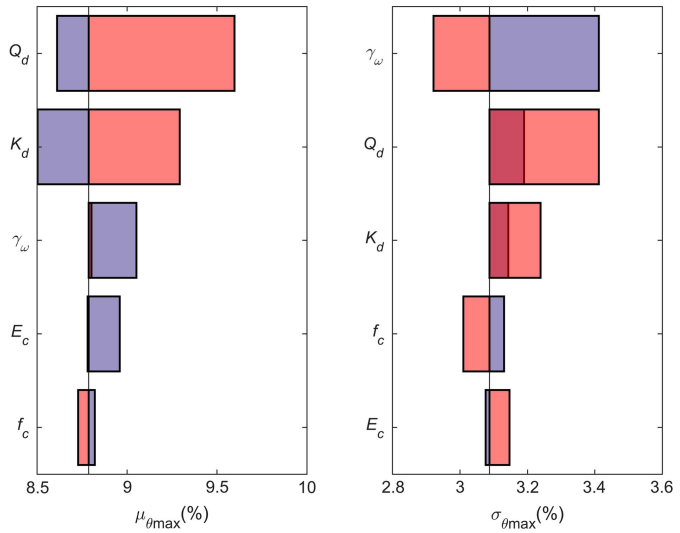

Fig. 8. Parameter sensitivities of the MDIL at design basic earthquake level.

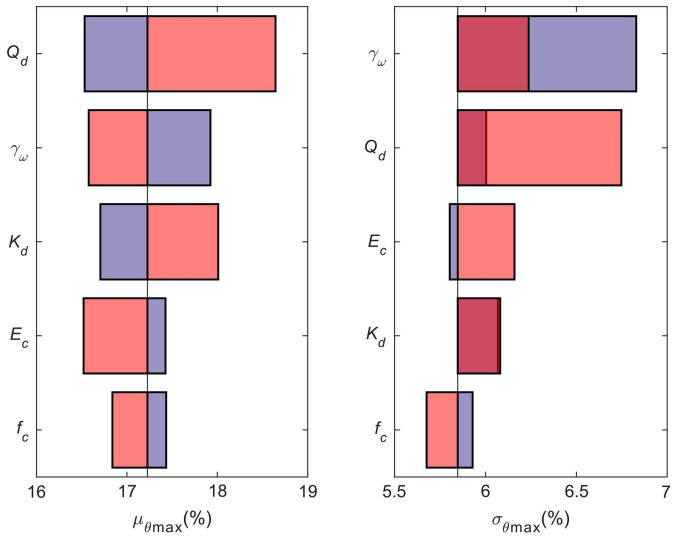

Fig. 9. Parameter sensitivities of the MDIL at severe earthquake level.

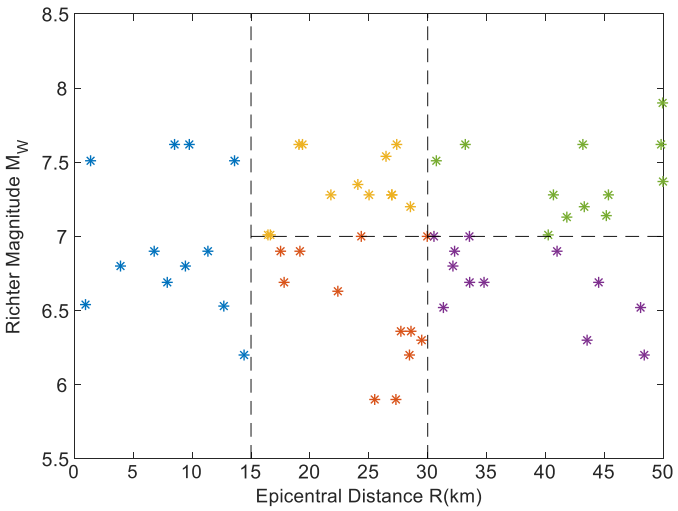

Fig. 10. Distribution of earthquake records selected by the bin method.

measure used in the seismic design code of China (MOHURD 2016) is the PGA. As a result, PGA is chosen as a seismic intensity measure and is constructed as an uncertainty parameter in response surface models. To fully consider the uncertainties in earthquake loadings, use 60 ground acceleration records to analyze the seismic fragility. The ground motions are actual records and are selected to meet the following criteria (Faravelli 1989; Rajashekhar and Ellingwood 1993): (1) the epicentral distance is less than 50 km, (2) the Richter magnitude of the selected database ranges from 5.5 to 9.0, (3) the site conditions are consistent with the structure located site, and (4) try to avoid the records coming from the same event. The bin method (Wong 1985) is adopted to classify and select the ground acceleration records. The Richter magnitude is used as a criterion to distinguish minor and major earthquakes, and the epicenter distance is used to judge near- and far-field earthquakes. The records' selection range is divided into five bins, as seen in the five rectangles in Fig. 10. Each bin's median spectral acceleration value is compared with the seismic design code to examine the representativeness of selected earthquake records. The response spectrums of 60 records from NGA-West2 are plotted in Fig. 11.

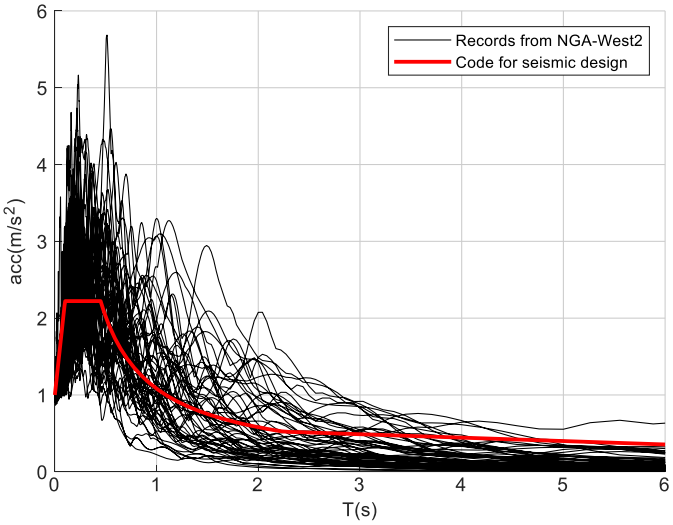

Fig. 11. Response spectrum of records from NGA-West2 and determined by the code for seismic design.

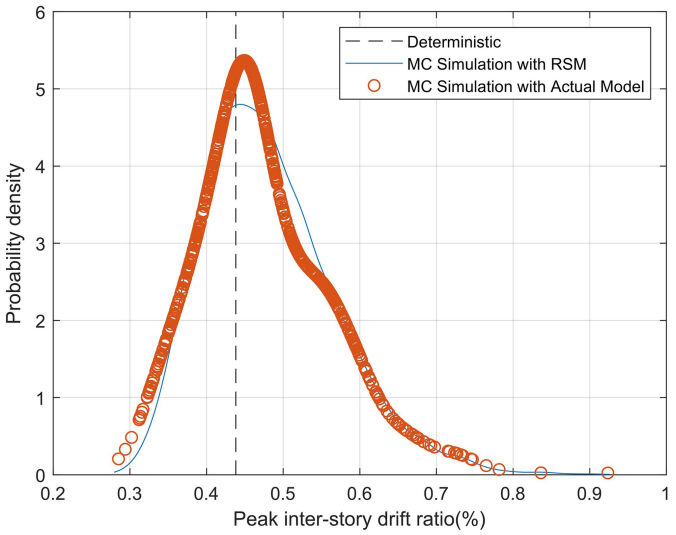

Fig. 12. Probability distribution of the PIDR.

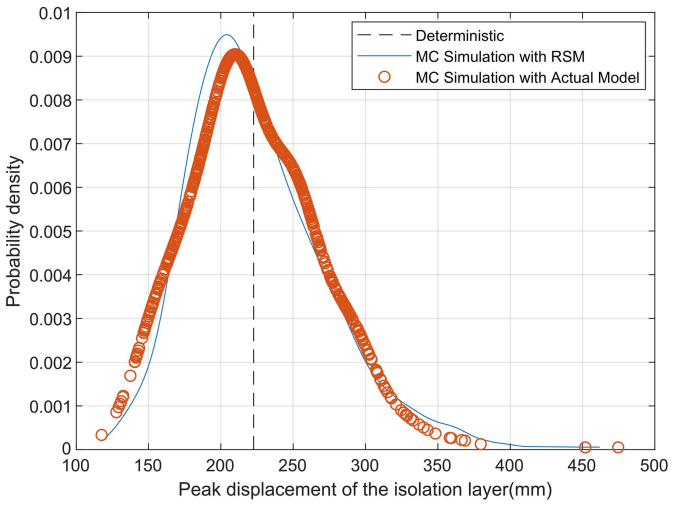

Fig. 13. Probability distribution of the MDIL.

Response Surface Models of the Base-Isolated Structure

It is more convenient to use normalized input variables in the experimental design domain instead of actual input variables. Assuming that each real input variable x_i has the definition domain $[x_{i,high}, x_{i,low}]$, its corresponding normalized design variable ξ_i can be calculated as

$$\xi_i = \frac{x_i - \frac{x_{i,high}+x_{i,low}}{2}}{\frac{x_{i,high}-x_{i,low}}{2}} \tag{12}$$

where $x_i = i$th random variable; ξ_i = corresponding normalized value of ith random variable; $x_{i,high}$ = upper bound of ith random variable; and $x_{i,low}$ = lower bound of ith random variable.

The structural random variables' design domain is converted to $[-1, 1]$, and their corresponding lower bound, center point, and upper bound are -1, 0, and 1, respectively. When dealing with the uncertainty of ground motions, the lower bound, the center point, and the upper bound correspond to the seismic intensity levels of minor, basic, and severe earthquakes, respectively. Divide 60 ground acceleration records into three batches. Then, scale the PGA of each batch to 1.1 m/s^2, 3.0 m/s^2, and 5.1 m/s^2, respectively. The CCD method designed a total of 43 sets of experimental designs for five random variables. Perform nonlinear dynamic time-history analysis at each design point value. Each design point corresponds to 20 ground acceleration records at a specific seismic intensity level. Obtain the PIDR and the MDIL at each design point and count their means and standard deviations. Then, use the least square method to fit the quadratic response surfaces of means and standard deviations of the metamodel representation [Eq. (6)], respectively. The response surface of the mean and standard deviation constitutes the response surface model of the PIDR and the MDIL. The response surface model of the PIDR is

$$\hat{y}_{\theta_{\max}} = \hat{y}_{\mu_{\theta_{\max}}}(PGA) + N[0, \hat{y}_{\sigma_{\theta_{\max}}}(PGA)] \tag{13}$$

and the response surface model of the MDIL is

$$\hat{y}_{\delta_{LRB}} = \hat{y}_{\mu_{\delta_{LRB}}}(PGA) + N[0, \hat{y}_{\sigma_{\delta_{LRB}}}(PGA)] \tag{14}$$

Testing and Validation of the Response Surface Model

To validate the response surface models, compare the calculation results of seismic response by direct MCS method and the RSM-based MCS method. The ground motion selected the Gazli strong motion record for this verification case and set the PGA to 0.52 g. When performing the direct MCS method, use the Latin hypercube sampling (LHS) method to generate 1,000 samples of structural input random variables, avoiding a mass of repeated sampling. Then, perform 1,000 times nonlinear dynamic time-history analysis and obtain the PIDRs and the MDILs. Figs. 12 and 13 compare the probability distributions of the PIDR and the MDIL by the LHS and RSM-based MCS methods. The black dashed lines in Figs. 12 and 13 are the seismic response for the deterministic analysis. Table 6 lists the statistical parameters of peak response quantities by two methods. The failure probability evaluated by two methods is further calculated, and the probability of a given limit state being exceeded is compared, as listed in Table 7. The cumulative probability density curves of the peak response quantities are also

Table 6. Statistical parameters of peak response quantities

Analysis method	PIDR			MDIL		
	Mean value (%)	Standard deviation (%)	Variable coefficient	Mean value (mm)	Standard deviation (mm)	Variable coefficient
MCS with RS model	0.48	0.09	5.60	225.52	48.13	4.69
Direct MCS	0.48	0.09	5.31	223.55	47.07	4.75

Table 7. Probability of a given limit state being exceeded

EDP	Failure probability	P_{LS_1}	P_{LS_2}	P_{LS_3}
PIDR	MC simulation with RS model	98.64	3.27	0.00
	Direct MCS	97.25	3.57	0.00
MDIL	MC simulation with RS model	75.66	23.91	0.44
	Direct MCS	76.24	25.96	0.27

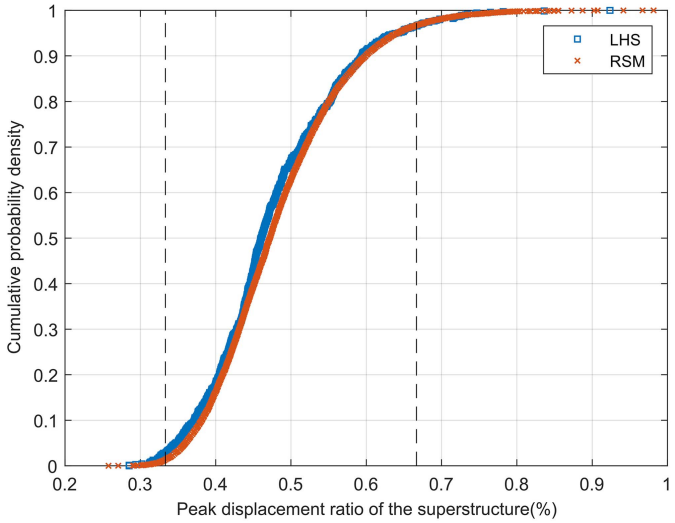

Fig. 14. Cumulative probability density curves of the PIDR.

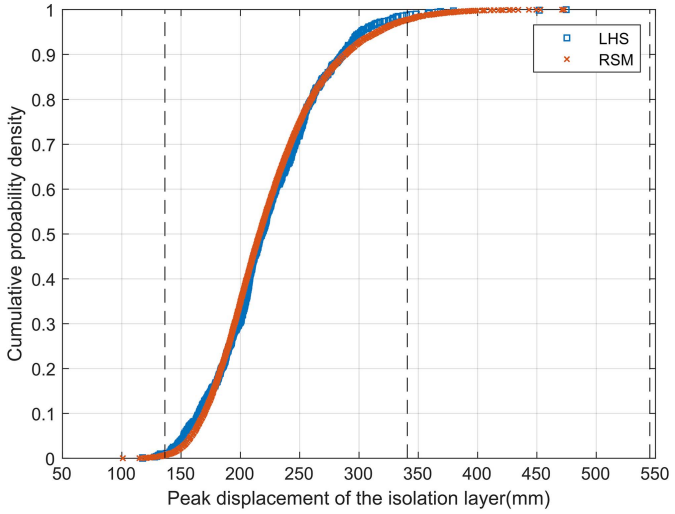

Fig. 15. Cumulative probability density curves of the MDIL.

compared and plotted in Figs. 14 and 15. The black dashed lines in Figs. 14 and 15 are the limit values of each limit state.

The calculated results of the RSM are in good agreement with the direct MCS method. However, the direct MCS requires 1,000 times nonlinear dynamic time-history analysis, whereas the RSM requires only 25 calculations. That indicates the time taken by the RSM is about 1/40 times that of the direct MCS method. It is evident that the RSM is much more efficient while maintaining accuracy.

Seismic Fragility Assessment of the Base-Isolated System

The failure of any part of the superstructure and the isolation layer will determine the failure of the whole structure so that the base-isolated structure can be considered a series system. According to probability theory, the failure event of a series system is the concatenation of the failure events of each subsystem. In other words, the failure probability of the base-isolated system is the concatenation of the failure probabilities of the superstructure and the isolation layer. So the failure event of the base-isolated system can be expressed as (Nielson and DesRoches 2007)

$$Fail_{system} = \bigcup_{i=1}^{n} Fail_{component-i} \tag{15}$$

where $Fail_{system}$ = failure event of the base-isolated system; and $Fail_{component-i}$ = failure event of ith structural component.

Cornell (Kounias 1968; Nielson and DesRoches 2007) proposed bounds of failure probabilities for series systems

$$\max_{i=1}^{n}[P(F_i)] \le P(F_{system}) \le 1 - \prod_{i=1}^{m}[1 - P(F_i)] \tag{16}$$

where $P(F_i)$ = failure probability of ith structural component; and $P(F_{system})$ = failure probability of the whole structural system. When the structural components are fully correlated, the failure probability of the structural system is equal to the maximum failure probability of each substructure $\max_{i=1}^{n}[P(F_i)]$, which is called the lower bound of the system's failure probability. When the structural components are independent of each other, the structural system's failure probability is equal to its upper bound $1 - \prod_{i=1}^{m}[1 - P(F_i)]$.

The response surface models constructed are used to calculate the base-isolated system's failure probabilities at each limit state, as listed in Table 8. The upper and lower bounds of the system's failure probability are also calculated. Define a variable Δ as

$$\Delta = \Delta_1 - \Delta_2 \tag{17}$$

where Δ_1 = failure probability of the actual system minus the lower bound; and Δ_2 = upper bound minus the failure probability of the actual system. $\Delta > 0$ indicates that the failure probability of the system is closer to the value of the upper bound; $\Delta < 0$ indicates that the failure probability of the system is closer to the value of the

Table 8. The failure probability of the base-isolated system

Limit states	P_{LS_1}	P_{LS_2}	P_{LS_3}
The failure probability of the base-isolated system	100.00	25.40	0.44
Upper bound	100.00	26.40	0.44
Lower bound	100.00	23.91	0.44
Δ	0.00	0.49	0.00

Table 9. The exceedance probability of the base-isolated system

Exceedance probability	P_{LS_1}	P_{LS_2}	P_{LS_3}
PGA = 0.1 g (minor earthquake)	0.01	0.00	0.00
PGA = 0.3 g (basic earthquake)	0.57	0.00	0.00
PGA = 0.5 g (severe earthquake)	0.93	0.11	0.00

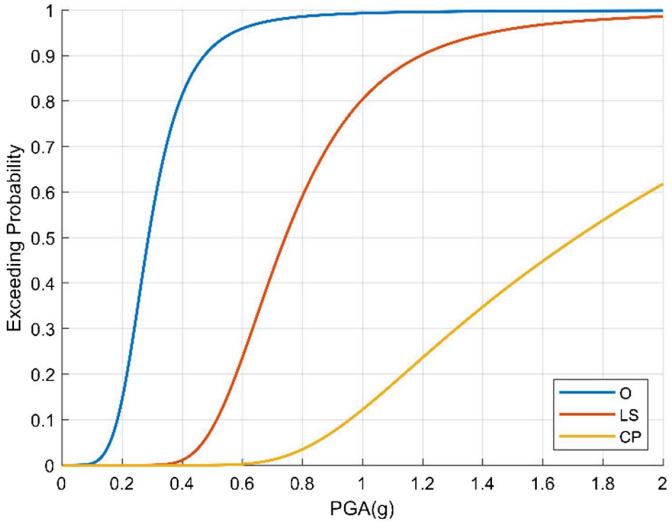

Fig. 16. Seismic fragility curves of the base-isolated system.

lower bound; and $\Delta = 0$ suggests that the failure probability of the system is in the middle range of the upper and lower bounds.

Table 8 documents that the failure probability of the base-isolated system is relatively close to the upper bound in Eq. (14). It indicates that the seismic responses of the superstructure and the base-isolation layer can be considered independent of each other. Therefore, the failure probability of the base-isolated system can be approximated by the following equation:

$$P(F_{system}) = 1 - \prod_{i=1}^{m}[1 - P(F_i)] \tag{18}$$

The failure probability of the base-isolated system exceeding each limit state is shown in Table 9. The seismic fragility curves of three limit states are plotted in Fig. 16.

Examining Table 9 and Fig. 16 reveals that the base-isolated structure will maintain operation under minor earthquakes, guarantee life safety under moderate earthquakes, and prevent collapse under severe earthquakes.

Damage State of the Base-Isolated Structure under Strong Earthquakes

The exceedance probability of the MDIL at large PGAs is calculated to investigate the isolators' performance under strong earthquakes, as shown in Table 10. When the PGA equals 0.6 g, the MDIL has a 10% probability of exceeding 250% shear strain; when PGA equals 0.7 g, the MDIL has a 19% probability of exceeding 250% shear strain and a 1% probability of exceeding 400% shear strain; when PGA equals 0.8 g, the MDIL has a 28% probability of exceeding 250% shear strain and a 4% probability of exceeding 400% shear strain. It indicates that the isolators may have a large displacement under the action of strong earthquakes. Therefore, it is significant to control the deformation of isolators within the allowable range, preventing them from exceeding the deformation capacity.

Table 10. The exceedance probability of the maximum displacement of the isolation layer

Exceedance probability	P_{LS_1}	P_{LS_2}	P_{LS_3}
PGA = 0.3 g	0.19	0.00	0.00
PGA = 0.4 g	0.41	0.00	0.00
PGA = 0.5 g	0.56	0.03	0.00
PGA = 0.6 g	0.66	0.10	0.00
PGA = 0.7 g	0.72	0.19	0.01
PGA = 0.8 g	0.76	0.28	0.04

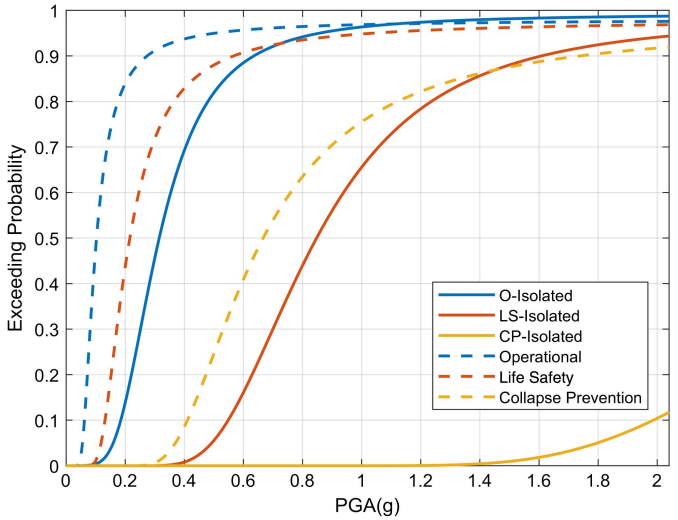

Fig. 17. Comparison of the seismic fragility curves of the base-isolated and nonisolated structures.

Comparison of Seismic Fragility of the Base-Isolated and Nonisolated Structures

The seismic fragility of the nonisolated counterpart is also analyzed for comparison purposes. The uncertainty parameters of the nonisolated structure selected are the concrete elastic modulus, bulk density, and PGA. Statistical descriptions of the random variables are the same as the base-isolated structure, and the random variables are assumed independent of each other. Ground acceleration records used for nonlinear analysis are consistent with the base-isolated one. The PIDR is identified as the demand parameter to compare two structures. Fig. 17 shows the fix-based and base-isolated structure's seismic fragility curves of three limit states.

It is concluded from Fig. 17 that the failure probabilities at various intensity levels are significantly reduced after base isolation. Moreover, the decrement of failure probability is more significant for higher damage levels, indicating that base isolation can effectively prevent the superstructure from entering a serious damage state.

Conclusion

This study proposed an RSM-based simulation approach to assess the seismic fragility of base-isolated structures. Uncertainties of base-isolated structures and ground motions were incorporated into the RSM-based approach. The uncertainty of ground motions was fully considered in the RSM-based approach by two means: selecting quantitative ground motions by the bin method and incorporating seismic intensity as an uncertain parameter. This study also compared the RSM-based MCS method with the traditional MCS method. It showed that the RSM could effectively reduce the computing workload of seismic fragility analysis while providing acceptable accuracy.

Three performance levels of base-isolated reinforced concrete structures were defined: operational, life safety, and collapse prevention. The PIDR of the superstructure and the MDIL were used to divide the limit states. Parameter sensitivity analysis was performed to study the uncertainty parameters that most influence the seismic responses of base-isolated structures. The sensitivity analysis showed that the concrete elastic modulus, the bulk density, the isolators' yield strength, and the isolators' postyield stiffness were the most influential parameters on the PIDR and the MDIL.

Moreover, a simplified seismic fragility evaluation method for seismic isolation systems was studied. It indicates that the seismic responses of the superstructure and the base-isolation layer can be considered independent of each other. Therefore, the failure probability of the base-isolated system can be approximated by the upper bound equation, that is, the base-isolated system can be considered a tandem system.

An actual RC structural project was taken as an example to illustrate the proposed approach and to study the effects of the base isolation technique. The dual response surface models were constructed, incorporating the uncertainty parameters of the base-isolated structure and the ground motions. The seismic fragility analysis results of the base-isolated system indicated that the base-isolated structure could achieve the performance objectives of maintaining operation under minor earthquakes, guaranteeing life safety under moderate earthquakes, and preventing collapse under severe earthquakes. Furthermore, the damage probabilities of the base-isolated structure beyond design intensity levels were discussed. The results showed that the seismic isolation bearings still had the possibility of large displacement under strong earthquakes. Thus, restraint devices or rubber buffers can be installed around the base isolation structure to prevent excessive displacement of the isolators. But the displacement limiting device needs to be investigated in detail to understand the impact on the structure's response. Last, the results of the seismic fragility analysis of the base-isolated and nonisolated structures showed that the base isolation technique significantly reduced the damage probability of the superstructure under various intensity levels and effectively prevented the superstructure from entering a serious damage state. The engineering example provided a reference for the fragility analysis of similar RC structures.

This study proved that the proposed RSM-based seismic fragility assessment approach provided high engineering application value. However, the research sample of this paper is limited, and more uncertainty parameters and structural forms will be discussed in the following research.

Data Availability Statement

All data, models, or code that support the findings of this study are available from the corresponding author upon reasonable request.

Acknowledgments

This study was funded by the independent projects for State Key Laboratory of Mechanical Behavior and System Safety of Traffic Engineering Structures (Grant Nos. ZZ2020-04 and ZZ2021-03), the Natural Science Foundation of Hebei Province (CN) (Grant Nos. E2019210245 and E202210095), and S&T Program of Hebei (CN) (Grant No. 21375407D).

References

Alhan, C., and H. P. Gavin. 2005. "Reliability of base isolation for the protection of critical equipment from earthquake hazards." *Eng. Struct.* 27 (9): 1435–1449. https://doi.org/10.1016/j.engstruct.2005.04.007.

ASCE. 1980. *Building code requirement for minimum design loads in buildings and other structures*. ANSI A58. Washington, DC: Dept. of Commerce, National Bureau of Standards.

ASCE. 2014. *Seismic evaluation and retrofit of existing buildings*. ASCE/SEI 41-13. Reston, VA: ASCE.

Box, G. E., and K. B. Wilson. 1951. "On the experimental attainment of optimum conditions." *J. R. Stat. Soc. B* 13 (1): 1–38.

Buratti, N., B. Ferracuti, and M. Savoia. 2010. "Response surface with random factors for seismic fragility of reinforced concrete frames." *Struct. Saf.* 32 (1): 42–51. https://doi.org/10.1016/j.strusafe.2009.06.003.

Castaldo, P., B. Palazzo, and P. Della Vecchia. 2015. "Seismic reliability of base-isolated structures with friction pendulum bearings." *Eng. Struct.* 95 (Jul): 80–93. https://doi.org/10.1016/j.engstruct.2015.03.053.

Celik, O. C., and B. R. Ellingwood. 2010. "Seismic fragilities for non-ductile reinforced concrete frames—Role of aleatoric and epistemic uncertainties." *Struct. Saf.* 32 (1): 1–12. https://doi.org/10.1016/j.strusafe.2009.04.003.

Faravelli, L. 1989. "Response-surface approach for reliability analysis." *J. Eng. Mech.* 115 (12): 2763–2781. https://doi.org/10.1061/(ASCE)0733-9399(1989)115:12(2763).

Franchin, P., A. Lupoi, P. E. Pinto, and M. I. Schotanus. 2003. "Seismic fragility of reinforced concrete structures using a response surface approach." *J. Earthquake Eng.* 7 (spec01): 45–77. https://doi.org/10.1080/13632460309350473.

GAQSIQ (General Administration of Quality Supervision, Inspection and Quarantine of the People's Republic of China). 2006. *Rubber bearings—Part 3: Elastomeric seismic-protection isolators for buildings*. GB/T20688.3-2006. Beijing: GAQSIQ.

Han, R., Y. Li, and J. van de Lindt. 2014. "Seismic risk of base isolated non-ductile reinforced concrete buildings considering uncertainties and mainshock–aftershock sequences." *Struct. Saf.* 50 (Sep): 39–56. https://doi.org/10.1016/j.strusafe.2014.03.010.

Kounias, E. G. 1968. "Bounds for the probability of a union, with applications." *Ann. Math. Stat.* 39 (6): 2154–2158. https://doi.org/10.1214/aoms/1177698049.

Kwon, O.-S., and A. Elnashai. 2006. "The effect of material and ground motion uncertainty on the seismic vulnerability curves of RC structure." *Eng. Struct.* 28 (2): 289–303. https://doi.org/10.1016/j.engstruct.2005.07.010.

Li, J., and J. B. Chen. 2004. "Probability density evolution method for dynamic response analysis of structures with uncertain parameters." *Comput. Mech.* 34 (5): 400–409. https://doi.org/10.1007/s00466-004-0583-8.

Long, X. H., J. Fan, B. B. Yang, and B. L. Chen. 2015. "Seismic fragility analysis of an isolated continuous girder bridge using the response surface method with random factors." *Adv. Struct. Eng.* 18 (12): 2059–2073. https://doi.org/10.1260/1369-4332.18.12.2059.

Mishra, S. K., and S. Chakraborty. 2013. "Performance of a base-isolated building with system parameter uncertainty subjected to a stochastic earthquake." *Int. J. Acoust. Vibr.* 18 (1): 7–19. https://doi.org/10.20855/ijav.2013.18.1315.

MOHURD (Ministry of Housing and Urban-Rural Development of the People's Republic of China). 2016. *Code for seismic design of buildings*. GB50011-2010. Beijing: MOHURD.

Nielson, B. G., and R. DesRoches. 2007. "Seismic fragility methodology for highway bridges using a component level approach." *Earthquake Eng. Struct. Dyn.* 36 (6): 823–839. https://doi.org/10.1002/eqe.655.

Peeranan, T. 2004. *Building seismic fragilities using response surface meta-models*. Atlanta: Georgia Institute of Technology.

Perotti, F., M. Domaneschi, and S. De Grandis. 2013. "The numerical computation of seismic fragility of base-isolated nuclear power plants buildings." *Nucl. Eng. Des.* 262 (Sep): 189–200. https://doi.org/10.1016/j.nucengdes.2013.04.029.

Rajashekhar, M. R., and B. R. Ellingwood. 1993. "A new look at the response surface approach for reliability analysis." *Struct. Saf.* 12 (3): 205–220. https://doi.org/10.1016/0167-4730(93)90003-J.

Saha, S. K., V. Matsagar, and S. Chakraborty. 2016. "Uncertainty quantification and seismic fragility of base-isolated liquid storage tanks using response surface models." *Probab. Eng. Mech.* 43 (Jan): 20–35. https://doi.org/10.1016/j.probengmech.2015.10.008.

Salimi Firoozabad, E., B.-G. Jeon, H.-S. Choi, and N.-S. Kim. 2015. "Seismic fragility analysis of seismically isolated nuclear power plants piping system." *Nucl. Eng. Des.* 284 (Apr): 264–279. https://doi.org/10.1016/j.nucengdes.2014.12.012.

SAPRC (The Standardization Administration of the People's Republic of China). 2021. *Standard for seismic isolation design of building*. GB/T51408-2021. Beijing: SAPRC.

Wang, H., Z. Wang, C. Luo, S. Liu, and D. Weng. 2020. "Seismic vulnerability analysis of base-isolated structures based on response surface method." In *Proc., 17th World Conf. on Earthquake Engineering (17 WCEE)*. Sendai, Japan: National Information Centre of Earthquake Engineering at the Indian Institute of Technology in Kanpur.

Wong, F. S. 1985. "Slope reliability and response surface method." *J. Geotech. Eng.* 111 (1): 32–53. https://doi.org/10.1061/(ASCE)0733-9410(1985)111:1(32).

Xiao, Y., K. Ye, and W. He. 2020. "An improved response surface method for fragility analysis of base-isolated structures considering the correlation of seismic demands on structural components." *Bull. Earthquake Eng.* 18 (8): 4039–4059. https://doi.org/10.1007/s10518-020-00836-w.